Analysis of Far-Infrared Spectra of Antiferromagnetic $FeCO_3$

G. A. Prinz, D. W. Forester, and J. L. Lewis*
Naval Research Laboratory, Washington, D. C. 20375
(Received 7 March 1973)

The transmission spectrum of antiferromagnetic $FeCO_3$ has been investigated in the far-infrared region from 20 to 300 cm^{-1}, for temperatures from 4.2 to 70 K and in applied fields up to 90 kOe. Spectra were obtained from natural single crystals and high-purity synthetic powders. At 4.2 K, a sharp electronic transition (magnetic dipole) was observed at 112.5 cm^{-1}, exhibiting parallel and perpendicular splitting factors of 6.6 and 0, respectively. Its oscillator strength is $f = 2.1 \times 10^{-8}$. An additional weak electronic line is observed at 160 cm^{-1}. The details of these transitions and electronic Raman transitions observed by others are successfully described by the Fe^{2+} single-ion Hamilitonian $\mathcal{H} = R\lambda\vec{L}\cdot\vec{S} + R^2\zeta(L_z^2 - 2/3) + \mathcal{J}S_z$, where λ, ζ, and $\mathcal{J}$ are the spin-orbit, trigonal-field, and Ising-molecular-field parameters, respectively, and R is an "orbital-reduction" factor. The analysis yields values for these parameters of $R\lambda = 105$ cm^{-1}, $-R^2\zeta = 1506$ cm^{-1}, $R \approx 1$, and $\mathcal{J} = 19$ cm^{-1}. The observed far-infrared transitions are identified as being within the low-^5E spin-orbit manifold from the ground state ($M_J = -1$) to the two components of the $M_J = 0$ doublet. The temperature dependence of the 112.5-cm^{-1} transition is studied from 4.2 to 70 K, and its intensity is observed to drop sharply as the temperature is raised to the vicinity of $T_N = 38.4$ K. This behavior is compared to that of an Ising spin system. In addition, three phonons are observed at 186, 201, and 224 cm^{-1} and are identified as external E_u, A_{2u}, and E_u modes, respectively.

I. INTRODUCTION

Ferrous carbonate ($FeCO_3$) is a transparent antiferromagnet possessing strong uniaxial magnetic anisotropy.[1] Its magnetic properties arise predominantly from the effect of a cubic crystalline electric field with a trigonal distortion and spin-orbit coupling in the ^5D ground state of the Fe^{2+} ion.[2] From a single-ion crystal-field analysis of Fe^{2+} in this material the over-all splitting of the lowest spin-orbit manifold is expected to be about 400 cm^{-1}. Several optical transitions are allowed between states within this manifold and should appear in the far-infrared spectral region. In the present paper,[3] we report an infrared spectral study of $FeCO_3$ in the frequency range from 20 to 300 cm^{-1} for both relatively pure natural single crystals and pure synthetic-powder samples. The studies were performed as a function of magnetic field, optical polarization, and temperature. In Sec. II we discuss previous experimental work and properties of the material which justify the use of a single-ion Ising-model description. Section III is a discussion of the theoretical considerations used to formulate a quantum-mechanical description of the Fe^{2+} eigenstates in $FeCO_3$ and includes the effects of cubic-plus-trigonal crystalline field, spin-orbit coupling, external magnetic field, and exchange. The experimental results are presented in Sec. IV, and the theoretical treatment is applied to these results in Sec. V.

II. PREVIOUS EXPERIMENTAL WORK

Ferrous carbonate occurs in nature as the mineral siderite with a rhombohedral calcite structure and has the symmetry properties of the space group $D_{3d}^6 = R\bar{3}_c$,[4] as illustrated in Fig. 1. There are two Fe^{2+} ions per molecular unit cell, which has the dimensions $a_0 = 5.795$ Å and $\alpha = 47°45$ sec.[4] Each divalent iron ion occurs at the center of an octahedron having a compressional distortion along the crystal [111] direction and is coordinated to six carbonate radicals. The crystalline electric field on each Fe^{2+} ion is dominantly of cubic symmetry, with a smaller trigonal component. All Fe^{2+} crystal sites are equivalent and located at inversion

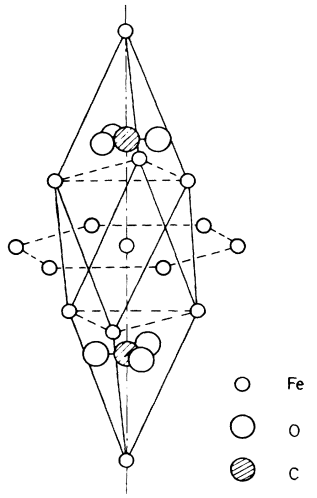

FIG. 1. Illustration of the crystal structure of $FeCO_3$. The vertical axis shown is the trigonal (C_3) axis and optic axis of the crystal. The central Fe^{2+} ion has six nearest neighbors, three in a plane above and three in a plane below as shown. The six-next-nearest neighbors lie in the plane containing the central ion.

centers along colinear threefold axes (C_3) which are parallel to the crystallographic c axis. Magnetic-susceptibility[1,5] and neutron-diffraction[6] studies at low temperatures have shown that the Fe^{2+} moments order antiferromagnetically. The magnetic moments point along the c axis. They lie in (0001) ferromagnetic sheets, and the successive sheets are antiferromagnetically aligned with one another. The six nearest (magnetic) neighbors (nn) to a given Fe^{2+} ion lie on the neighboring sheets, while the six second-nearest neighbors lie in the same sheet. Hence there is antiferromagnetic alignment between nearest neighbors and ferromagnetic alignment between second-nearest neighbors, yielding a two-sublattice description of the magnetic structure.

In an axial magnetic field of about 150 kOe at 4.2 K,[1,7] the antiferromagnetic coupling between nn can be overcome, producing a "metamagnetic" transition from the antiferromagnetic state to a ferromagnetic (saturated paramagnetic) state. Such a high critical magnetic field for $FeCO_3$ indicates that its near-neighbor coupling is large in comparison with other ferrous compounds. $FeCl_2$, for example, which has a similar crystal structure, has a critical field of only about 11 kOe.[8]

From Faraday rotation[7] and magnetization measurements[9] of $FeCO_3$ at fields extending above 290 kOe, as well as from high-temperature susceptibility[5] measurements, the magnetic moment per Fe^{2+} ion is deduced to be about $5.0\mu_B$.[9] The Néel temperature is determined to be 38.4 K.[10,11] Results of neutron-diffraction,[12] Mössbauer,[10,11,13] and magnetization[1] studies all show that the antiferromagnetic spin system of $FeCO_3$ behaves very much like that of three-dimensional Ising systems. Preliminary infrared-spectroscopy measurements by us[14] showed a magnetic excitation near 112 cm^{-1} whose temperature dependence of frequency and intensity is characteristic of an Ising spin system. Inelastic neutron scattering experiments[12] also show an excitation at 112 cm^{-1} for $\vec{k}=0$. These neutron experiments show that over most of the Brillouin zone this excitation has no dispersion, as expected for an Ising excitation.

Very little optical work has been done on $FeCO_3$. McClure *et al.*[15] have performed optical-transmission studies in the vicinity of 24 000–25 000 cm^{-1}, both above and below the 150-kOe metamagnetic transition field. They find a series of spectral features which they suggest may be magnon-exciton pairs. More recently, electronic Raman excitations have been observed[16,17] in $FeCO_3$ at 438 and 1743 cm^{-1} at 4.2 K.

III. THEORETICAL CONSIDERATIONS

The eigenstates of the Fe^{2+} ion in environments similar to that in $FeCO_3$ have been studied theoretically by Kanamori[2] in the single-ion crystal-field approximation. The energy-level splitting is shown schematically in Fig. 2. The free-ion ground term ^5D is split by the large cubic component of the crystal field into a doublet, ^5E at $+6Dq$, and a triplet, $^5T_2$, at $-4Dq$. The separation $10Dq$ is of the order of 10 000 cm^{-1}. The smaller trigonal-field potential[18]

$$V_T = aR_2(r)Y_2^0 + bR_4(r)Y_4^0 \tag{1}$$

separates the $^5T_2$ state into a singlet $^5A_1$ and a doublet ^5E. For a compressional trigonal distortion the doublet ^5E is predicted to be lowest and this has been verified by Mössbauer[10,11,13] studies. This result is also consistent with a magnetic moment of about $5\mu_B$ in the ground state. From these studies the separation ζ between the $^5A_1$ and ^5E states in $FeCO_3$ is predicted to be of the order of 1 000 cm^{-1}.[19] This may be contrasted with $\zeta = 88$ cm^{-1} in $FeCl_2$.[20] Spin-orbit interactions split the tenfold degenerate ^5E state and the fivefold degenerate $^5A_1$ state. The free-ion value of the coupling constant λ is ≈ 100 cm^{-1}.[2] The resultant spin-orbit manifold for the ^5E state will have an over-all splitting of about 400 cm^{-1}, and transitions within this manifold are in the far infrared.

Both the trigonal-field term in Eq. (1) and second-order spin-orbit interaction produce small admixtures of the ground ^5E state and the ^5E at $10Dq \cong 10\,000$ cm^{-1}. If these interactions, as well as term-mixing, are neglected then the $^5T_2$ state is equivalent to a ^5P state and can be treated as such. The basis functions which span the ^5P manifold are linear combinations of the fifteen $|M_S, M_L\rangle$ states, where $M_S = 0, \pm1$, and ±2 and $M_L = 0, \pm1$. It can be shown[21] that the equivalence is obtained by using these basis functions and by replacing the angular momentum operator $\vec{L}$ by $-\vec{L}$. The Hamil-

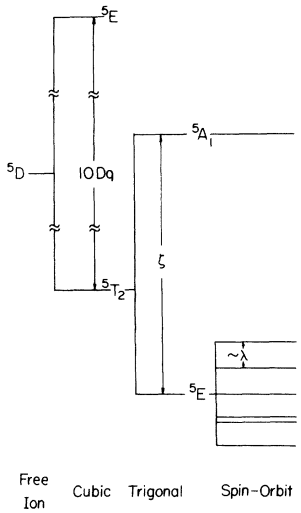

FIG. 2. Lowest free-ion term of Fe^{2+} in $FeCO_3$ split by cubic field with trigonal distortion and spin-orbit interaction ($10Dq \approx 10^4$ cm^{-1}, $\zeta \approx 10^3$ cm^{-1}, and $\lambda \approx 10^2$ cm^{-1}).

tonian to consider in the ^5P manifold for ion i is, then,

$$\mathcal{H}_i = \lambda R\vec{L}_i\cdot\vec{S}_i + \zeta R^2(L_{iz}^2-\tfrac{2}{3}) + \mu_B\vec{H}\cdot(-R\vec{L}_i+2\vec{S}_i)+\sum_j J_{ij}\vec{S}_i\cdot\vec{S}_j \ . \quad (2)$$

The first term in Eq. (2) is the spin-orbit interaction, where λ is the coupling constant. The second term is the trigonal-field potential in operator equivalent form for an $L=1$ state, where ζ is the strength of this interaction. The third term is the Zeeman coupling to an external magnetic field H and the last term is the pairwise magnetic exchange interaction of ion i with its neighbors. Because of covalency effects and mixing with the upper ^5E state, we have included a factor R (the "orbital reduction factor") representing a deviation of the maximum possible $\langle L_z\rangle$ from unity.

Griffith[21] has treated the eigenvalue problem for this Hamiltonian in the case of zero exchange and zero magnetic field with $R=1.0$. The 15×15 matrix of $\mathcal{H}$ [Eq. (2)] breaks up into 7 submatrices of which three are 3×3 (for $M_J=0,\pm1$), two are 2×2 ($M_J=\pm2$) and two are 1×1 ($M_J=\pm3$). We have extended Griffith's numerical calculations to larger values of ζ/λ and have added the exchange and magnetic field. To aid in understanding the solutions we will first examine a limiting case.

A. Limiting Case for $\zeta/\lambda\to-\infty$

In the limit $\zeta/\lambda\to-\infty$, the energies and wave functions for all fifteen ^5P states approach the values shown in Fig. 3. The lowest-lying states are five doubly degenerate levels of equal spacing $R\lambda$. The twofold degeneracy of these five low-lying levels is just time-reversal degeneracy, and will be lifted by a real or effective magnetic field. Fig. 3 illustrates this splitting as caused by an exchange field. The labels which indicate the compositions of the states in Fig. 3 are for ions on one sublattice. For those ions on the other sublattice, one applies time reversal which reverses the signs of all the momenta. Although the Hamiltonian is for Heisenberg (isotropic) exchange, it is clear from the compositions of the states, indicated in Fig. 3, that the crystalline anisotropy renders the exchange totally anisotropic (or Ising) to first order since the matrix elements of S_x and S_y are zero within the ground doublet. We can therefore write the exchange part of Eq. (2) as an effective Ising molecular field,

$$H_{ex}=\mathcal{J}S_{iz} \ . \quad (3)$$

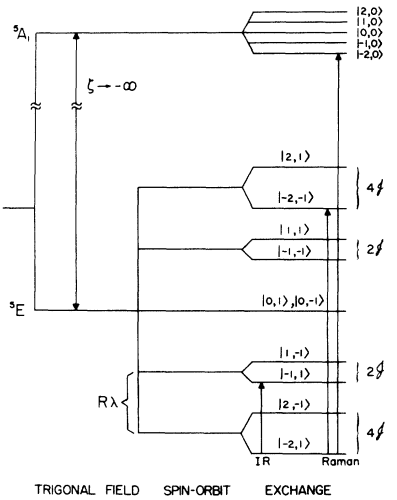

FIG. 3. Energies and compositions of the fifteen ^5P states in the limit $\zeta\to-\infty$, including the spin-orbit interaction $R\lambda$ and an Ising exchange field $\mathcal{J}$. The allowed infrared (IR) and Raman transitions are indicated.

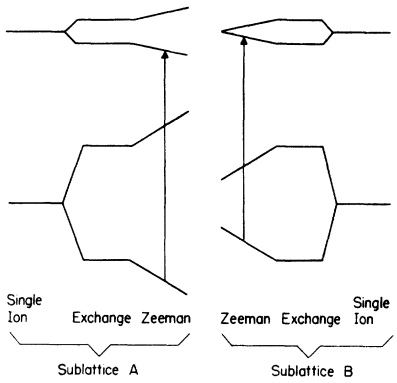

FIG. 4. Illustration of the pseudosplitting of an electronic transition in a two-sublattice antiferromagnet. The transitions involve ions on separate sublattices, but coincide in zero applied magnetic field.

Infrared transitions between levels in Fig. 3 are limited to magnetic dipole ($\Delta M_J=\pm1,0$) since the Fe^{2+} ions are at centers of inversion in the crystal. Raman transitions are governed by the selection rules $\Delta M_L=\pm2,\pm1$, and 0 and $\Delta M_S=0$. Thus, in the limit of infinite trigonal field, there is one infrared transition shown in Fig. 3 from the ground state $|-2,1\rangle$ ($M_J=-1$) to the state $|-1,1\rangle$ ($M_J=0$). The other lines in Fig. 3 indicate the two allowed Raman transitions. In an applied magnetic field along the z axis the observed absorption lines will show a pseudosplitting. Ions on one sublattice see their effective field enhanced so the doublet splittings are increased, while those on the other sublattice see their effective field diminished and their doublet splittings are decreased. Since the initial (i) and final (f) states of a given transition may have different magnetic splitting factors $g_{\parallel}$, the transition energy will, in general, decrease for one sublattice and increase for the other (see Fig. 4). Thus, in an axial magnetic field, a frequency ν_0

splits according to

$$\nu_{\pm} = \nu_0 \pm \tfrac{1}{2}(g_{\parallel}^{i} - g_{\parallel}^{f})\mu_B H \equiv \nu_0 \pm \tfrac{1}{2}\Delta g \mu_B H \quad . \tag{4}$$

Restricting our attention to the magnetic dipole transition, then for axial polarization (α) this would appear as two absorption lines, one right-hand circularly polarized, the other left-hand circularly polarized. The relevant splitting factors for each level are calculated using

$$g_{\parallel} \equiv 2\left|\langle M_L, M_S \left| -RL_z + 2S_Z \right| M_L, M_S\rangle\right|$$

or (5)

$$g_{\parallel} = 2\left|(-RM_L + 2M_S)\right|$$

In this extreme trigonal-field limit we obtain $g_{\parallel}^{i} = 10$ for the $|-2, 1\rangle$ state and $g_{\parallel}^{f} = 6$ for the $|-1, 1\rangle$ state so that $\Delta g \equiv (g_{\parallel}^{i} - g_{\parallel}^{f}) = 4$. The perpendicular g factors are zero to first order for this transition.

B. Case for $-\infty < \zeta/\lambda < 0$

The assumption of $\zeta/\lambda \to -\infty$ made thus far is, of course, extreme. When ζ/λ is reduced, one finds that the spin-orbit coupling causes a small amount of mixture between $|M_S, M_L\rangle$ states with the same $M_J = M_S + M_L$. These admixtures are indicated in Fig. 5. An important new feature to be noted is that while four of the five doublets are still degenerate, the first excited doublet, which was "accidentally" degenerate, is now split. Its eigenstates are the symmetric and antisymmetric pairs

$$\begin{aligned} \psi_1 &= \alpha\,|1, -1\rangle + \alpha\,|-1, 1\rangle + \epsilon\,|0, 0\rangle \quad , \\ \psi_2 &= a\,|1, -1\rangle - a\,|-1, 1\rangle \quad , \end{aligned} \tag{6}$$

where a small amount, ϵ, of $|0, 0\rangle$ is mixed into the symmetric state but not into the antisymmetric

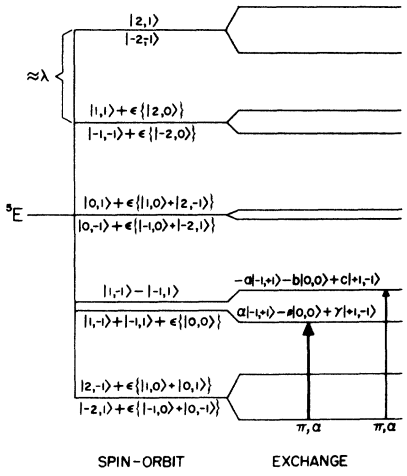

FIG. 5. Spin-orbit and Ising exchange field splitting of the low-lying ^5E multiplet of Fe^{2+} for a noninfinite value of the trigonal field term ζ/λ. The allowed infrared transitions and their polarizations are indicated.

TABLE I. Illustration of the dependence of the composition of the states ψ_1 and ψ_2 of the $M_J = 0$ doublet on the ratios ζ/λ and $\mathcal{J}/\lambda$, with $R \approx 1$, $\lambda \approx 100$ cm^{-1}, and where $\psi_1 = \alpha\,|-1, 1\rangle - \beta\,|0, 0\rangle + \gamma\,|1, -1\rangle$ and $\psi_2 = -a\,|-1, 1\rangle - b\,|0, 0\rangle + c\,|1, -1\rangle$.

$-\zeta/\lambda$	$\mathcal{J}/\lambda$	α	β	γ	a	b	c
10	0	0.69	0.22	0.69	0.71	0	0.71
10	0.1	0.83	0.22	0.59	0.53	0.06	0.85
20	0	0.70	0.13	0.70	0.71	0	0.71
20	0.1	0.91	0.12	0.39	0.40	0.05	0.92
∞	0	0.71	0	0.71	0.71	0	0.71
∞	0.1	1.0	0	0	0	0	1.0

state. This admixture is the cause of the zero-field splitting. Note that magnetic dipole transitions are allowed between the ground state and both components of this zero-field doublet.

The addition of exchange or magnetic field significantly mixes the wave functions ψ_1 and ψ_2 in Eq. (6). With increasing $\mathcal{J}$ or H, these states tend to purify to $|1, -1\rangle$ and $|-1, 1\rangle$ which are just the eigenstates of the exchange (or magnetic field) terms alone. As we shall see, the exchange energy is comparable to the crystal-field splitting of this $M_J = 0$ doublet and the resulting state compositions (and thus the energies and g factors) are strongly dependent on $\mathcal{J}$ (or H) as well as on ζ/λ. This dependence is illustrated in the tabulation of coefficients in Table I.

IV. EXPERIMENTAL PROCEDURES AND RESULTS

A. Experimental Procedures

The far-infrared absorption spectra of $FeCO_3$ were obtained using a commercially available interferometric spectrometer.[22] This instrument is of the Michelson type employing a Mylar beam splitter. The interferograms were taken over a path difference of 1 cm as measured from the zero path. This provided data points in the Fourier transform which were spaced 0.5 cm^{-1} apart. Under ideal conditions of signal to noise, this represents a spectral resolution of 1.0 cm^{-1}. An InSb detector[23] operated at 4.2 K was used to study the spectral region between 20 and 80 cm^{-1}. A Ga-doped germanium photoconductor, operated at 4.2 K, was used from 80 cm^{-1} to its high-energy limit of about 300 cm^{-1}. In addition to the interferometer, the experiment employed a superconducting solenoid capable of providing 90 kOe. Radiation from the interferometer is conducted via evacuated light pipes down through the bore of the solenoid to the photodetector. The sample is placed in the light pipe at the solenoid center. The section of light pipe containing sample and detector is enclosed in a separate evacuable container which is sealed by a polyethylene window. This container, inserted through the bore of the solenoid and immersed in the liquid He used to cool it, is filled

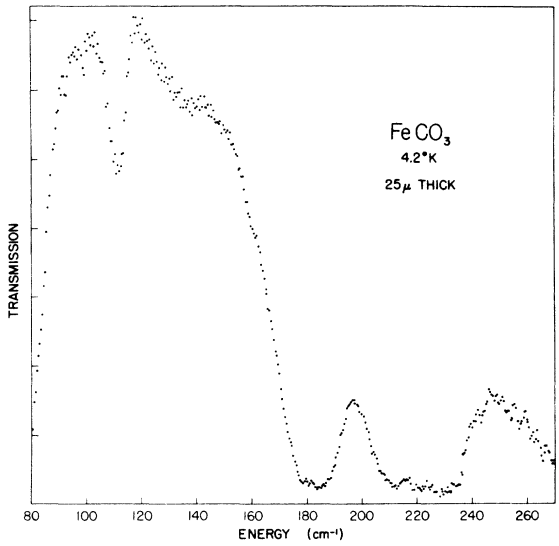

FIG. 6. Transmission spectrum of a single-crystal sample of $FeCO_3$, 25 μm thick, in α polarization. The sharp decline at 80 cm^{-1}, the gradual decline at high energies, and the feature at 140 cm^{-1} are due to the detector response. The line at 112.5 cm^{-1} and the shoulder at 160 cm^{-1} are electronic transitions. The strong absorption lines at 186 and 224 cm^{-1} are phonons.

with He exchange gas which cools both sample and detector via conduction.

Since synthetic single crystals large enough for transmission spectroscopy are not yet available, the single-crystal samples studied were cut from natural crystals of siderite, obtained from deposits in Quebec. To obtain the very thin samples required for transmission studies, sections were cut from x-ray-oriented faces, glued to substrates, and then polished down to the required thickness. The substrates were either Mylar or high-purity silicon. Sample mounts providing various orientations and linear polarizers placed just before the sample allowed spectra to be obtained in which (i) the radiation propagated parallel to the trigonal axis (α polarization) and (ii) the radiation propagated perpendicular to the trigonal axis with either $\vec{E}_{\parallel} C_3$ (π polarization) or $\vec{E} \perp C_3$ (σ polarization). The magnetic field was applied either parallel to the trigonal axis (to measure $g_{\parallel}$) or perpendicular to the trigonal axis (to measure $g_{\perp}$).

Natural crystals suffer from variations in their chemical composition. A spectrochemical analysis on different sections from which the slices were taken showed as little as 0.01-at.% or as much as 4-at.% manganese impurity. The distributions of these impurities are by no means uniform so that adjacent sections from the same specimen showed differences in their transmission spectra. Sections were carefully chosen to minimize contributions from these impurity effects.

For polarization and Zeeman studies, single crystals were required. For the temperature dependence studies, however, a powder sample was adequate and a high-purity synthetic-powder sample[24] was used. This powder was dissolved in molten polyethylene and pressed into a brass holder which was wrapped with heater wire.

The holder and sample were cooled by the exchange gas which was in contact with a 4.2-K reservoir. The temperature was determined by a Au-Chromel thermocouple attached to the brass holder next to the sample. In retrospect, some way of imbedding the thermocouple in the pellet would have been desirable since there was a possibility of temperature difference between the thermocouple and sample. The poor thermal conductivity of polyethylene probably created a temperature gradient across the pellet, the edges being the temperature of the brass mount and the center being cooler.

This difficulty will be referred to in the later discussion of the temperature dependence.

B. Experimental Results

A typical transmission spectrum of a 25-μm-thick single-crystal sample taken in α polarization at 4.2 K is shown in Fig. 6 for the spectral region 80–300 cm^{-1}. In this figure, the spectral response of the Ga-doped germanium detector has not been ratioed out. The absorption spectrum is dominated above about 180 cm^{-1} by strong lattice absorption. The broad feature at about 140 cm^{-1} is characteristic of our detector and disappeared upon ratioing. A sharp absorption line at 112.5 cm^{-1} is noted and is found to be magnetic in character. It is observed with equal strength in π and α polarization, but it is absent in σ polarization, indicating that it is a magnetic dipole (MD) transition.

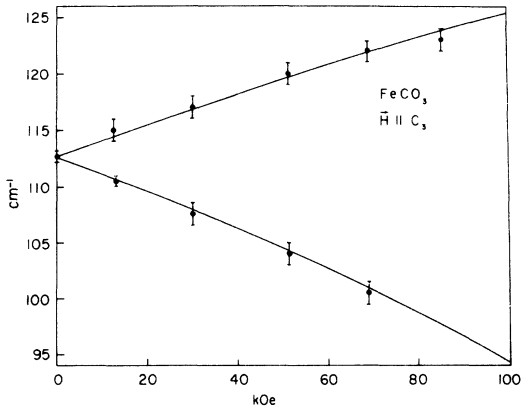

FIG. 7. Zeeman splitting of the 112.5-cm^{-1} transition in an external magnetic field applied parallel to the optic axis of $FeCO_3$. The smooth curve is calculated using the parameters given in the text.

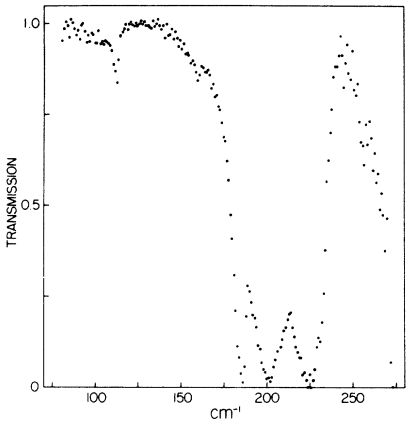

FIG. 8. Transmission spectrum of synthetic $FeCO_3$ dissolved in polyethylene, equivalent to a 1-μm-thick single crystal. The three absorption lines at 186, 201, and 224 cm^{-1} are independent of temperature and magnetic field and are identified as phonons. The line at 201 cm^{-1} is absent in α polarization (Fig. 6).

This line exhibits no splitting in magnetic fields up to 90 kOe applied perpendicular to the C_3 axis. In fields applied parallel to the C_3 axis the line Zeeman splits as illustrated in Fig. 7. Although there is some departure from linearity at high fields, at zero field each component moves at a rate of about 0.15 cm^{-1} kOe. Since this reflects the combined Zeeman splitting of the initial and final state, we obtain, using Eq. (4),

$$\Delta E/\Delta H = \tfrac{1}{2}\mu_B \Delta g_{\parallel} = 0.15 \pm 0.005 \text{ cm}^{-1}/\text{kOe}$$

or

$$\Delta g_{\parallel} = 6.6 \pm 0.2 \ .$$

The line at 112.5 cm^{-1} is the only spectral feature which exhibits any observable temperature dependence in the range 4.2–70 K. At 4.2 K its full linewidth at half-maximum is 7 cm^{-1} and the line remains unchanged as the temperature is raised from 4.2 K until approximately 28 K. Above this temperature the line gets progressively weaker and broadens until it finally merges with the background near $T_N \approx 38$ K. There is no noticeable shift in position, however. A detailed discussion of the temperature dependence is given in Sec. V. The polarization, characteristic Zeeman splitting, and temperature dependence of this line lead us to interpret it as a single-ion excitation of Fe^{2+}, as indicated in Fig. 5, between the $M_J = -1$ ground state and the next $M_J = 0$ level above.

TABLE II. Summary of experimentally determined frequencies (cm^{-1}) of the external ($\vec{k}=0$) phonons in $FeCO_3$. Out of a possible ten phonons ($2A_{2u}+3E_u+2E_g+A_{1u}+2A_{2g}$) six have been observed.

ir active		Raman active		Silent	
185[a]	E_u	186[b]	E_g	269[a]	A_{2g}
186[c]					
201[c]	A_{2u}	287[b]	E_g		
224[c]	E_u				

[a]Reference 12. [b]Reference 16. [c]This work.

Additional spectral features are better illustrated in Fig. 8, which shows the region 80–300 cm^{-1} obtained from a powder sample dissolved in polyethylene with a path length equivalent to a crystal approximately 1 μm thick. For this unpolarized spectrum, the detector response has been ratioed out. In addition to the sharp MD transition at 112 cm^{-1} there is a weak sharp line at 160 cm^{-1} which can be seen only as a shoulder on the strong phonon absorption in Fig. 6. There is also a possible line near 256 cm^{-1}, although here the poor signal to noise caused by the deteriorating detector response makes reliable identification difficult. For the thinnest single crystals obtained, these weak lines are masked by the phonon absorption and their response to magnetic fields and temperature could not be followed. We identify as phonons the three absorption lines at 186, 201, and 224 cm^{-1}. The line at 201 cm^{-1} was absent in α polarization as shown in Fig. 6.

By comparison with other carbonates, the $\vec{k}=0$ phonons associated with internal vibrational modes are much higher than 300 cm^{-1}. We therefore need consider only the external vibrations whose symmetries in the calcite structure are $A_{1u}+2A_{2u}+3E_u+2A_{2g}+2E_g$. Five of these are ir active ($2A_{2u}+3E_u$) and two are Raman active ($2E_g$). The available experimental data on these external modes in $FeCO_3$ from various sources is summarized in Table II. The 186-, 201-, and 224-cm^{-1} lines are identified as E_u, A_{2u}, and E_u, respectively, from our observed polarizations and by comparison with isomorphic $CaCO_3$ and $MgCO_3$.[25] Figure 8 also indicates strong absorption setting in near 280 cm^{-1}, just below the limit of our equipment. This agrees with the expected location of the remaining A_{2u} and E_u ir modes which are found in this region in $CaCO_3$ and $MgCO_3$.

Using both powder samples and single crystals, spectra were also taken from 20 up to 80 cm^{-1}, but no additional excitations were observed.

V. ANALYSIS

A. Determination of Parameters

In Secs. II and III we discussed experimental and theoretical justification for treating the Fe^{2+} ion in $FeCO_3$ in terms of a single-ion picture with an Ising exchange field. With these assumptions we may solve the Hamiltonian of Eq. (2) using the experimental data to obtain a quantum-mechanical

description of the Fe^{2+} ion in this material. The data consists of the two ir transitions indicated in Fig. 5 and of the two Raman transitions indicated in Fig. 3. An analytic solution of the matrix for the Hamiltonian [Eq. (2)], carried to first order in $(R\lambda)^2/R^2\zeta \equiv \Delta$, gives, as the approximate expressions for the measured energies of these transitions,

$$\left.\begin{aligned} &112.5 \pm 0.5\ \text{cm}^{-1} \cong R\lambda - 4\Delta + 2\mathcal{J} && (7a)\\ &160 \pm 1\ \text{cm}^{-1} \cong R\lambda + 2\Delta + 2\mathcal{J} && (7b)\end{aligned}\right\}\ \text{(ir)},$$

$$\left.\begin{aligned} &438 \pm 2\ \text{cm}^{-1} \cong 4R\lambda + 2\Delta && (7c)\\ &1743 \pm 2\ \text{cm}^{-1} \cong R^2\zeta + 2R\lambda + 4\Delta && (7d)\end{aligned}\right\}\ \text{(Raman)},$$

where we have assumed the same exchange $\mathcal{J}$ for all electronic states.

If we solve Eqs. (7a)–(7d) for the variables, we obtain $R^2\zeta \cong -1500\ \text{cm}^{-1}$, $R\lambda \cong 106\ \text{cm}^{-1}$, $\mathcal{J} \cong 19\ \text{cm}^{-1}$, and $\Delta \cong 8\ \text{cm}^{-1}$.

We see that $(R\lambda)^2/(R^2\zeta) = 7.5$ is indeed in reasonable agreement with the value for Δ.

These values for the trigonal-field, spin-orbit, and exchange parameters are about what one would expect from the discussion in Sec. IV and the Appendix and indicate that the picture is reasonable.

If one now proceeds to reproduce the observed Zeeman behavior of the 112.5-cm^{-1} transition, its extreme sensitivity to the parameter values necessitates an exact numerical computer analysis of the 15×15 secular determinant of $\mathcal{H}$ in Eq. (2). A search for a set of parameters which will provide an acceptable fit to the data quickly reveals that the requirement of keeping the exchange constant $\mathcal{J}$ the same for all the electronic states is too severe. In particular, it will not permit one to simultaneously obtain both the 112.5-cm^{-1} energy and its splitting factor of 6.6. A relaxation of that requirement, i.e., allowing a different exchange constant for the first excited doublet ($\mathcal{J}_1$ for $M_J = 0$ and $\mathcal{J}_0$ for all others), permits one to very easily obtain a good fit. This is illustrated in Table III where the experimental values are compared with those obtained for a range of parameter values. It is interesting to note that good results are obtained for a large range of R, but a relatively narrow range for $R\lambda$, $R^2\zeta$, $\mathcal{J}_0$, and $\mathcal{J}_1$. The large range in R merely arises from the fact that R and $\mathcal{J}_1$ may be mutually adjusted to give the observed Zeeman behavior. To obtain unique values of R, λ, and ζ, $\Delta g_{\parallel}$ must be determined to very high precision.

Although the low-temperature energy levels are reproduced quite well with the parameters in Table III, there is a problem in explaining the temperature dependence of the 438-cm^{-1} Raman transition.[16,17] Both of these studies show a shift to higher energies as the temperature is raised from 4.2 K up through the Néel temperature ≈ 39 K. This can only be true if the upper-state exchange splitting ($\mathcal{J}_2$) exceeds that of the ground state. This is in disagreement with our calculated result which would require the excited-state exchange splitting to be slightly smaller than the ground state. The temperature dependence of the 112.5-cm^{-1} transition is discussed in detail in Sec. V C.

TABLE III. A comparison of the calculated and observed splitting factors and transition energies for several values of the parameters in Eq. (2). All energies are in cm^{-1}.

Observed	Calculated				
6.6 ± 0.2	6.70	6.69	6.67	6.65	6.63
112.5 ± 0.5	112.36	112.40	112.42	112.43	112.46
160 ± 1	160.4	160.3	160.2	160.2	160.1
438 ± 2	431	432	434	435	437
1743 ± 2	1747	1747	1746	1745	1744
	Parameters				
R	1.2	1.1	1.0	0.9	0.8
$R\lambda$	104.4	104.5	105.1	105.4	105.8
$R^2\zeta$	1509.5	1508.1	1506.4	1504.7	1502.9
$\mathcal{J}_0$	19.2	19.0	18.9	18.7	18.5
$\mathcal{J}_1$	13.8	13.5	13.2	12.9	12.5

A point that has been ignored in this analysis is electron-phonon interactions for these low-lying states. The existence of phonons in the 180–230-cm^{-1} region and at ≈ 300 cm^{-1} has been established. Neutron-diffraction studies of the 112.5-cm^{-1} transition show electron-phonon coupling effects occurring near the zone boundary. It would be of interest to see if there are similar effects near zone center for the other phonons.

B. Oscillator Strength

The strength of the 112.5-cm^{-1} transition provides an additional experimental check on the identification of the transition. The oscillator strength for a magnetic dipole transition between states i and f is given by

$$f_m = \left(\frac{8\pi^2 mc}{3he^2}\right)\tilde{\nu}n\left|\frac{e\hbar}{2mc}\langle f|\vec{L}+g_s\vec{S}|i\rangle\right|^2,$$

where $\tilde{\nu}$ is the transition frequency in cm^{-1} and n is the index of refraction at $\tilde{\nu}$. Because of our use of an effective ^5P Hamiltonian, we replace $\vec{L} \to -\vec{L}$. The transition at 112.5 cm^{-1} is polarized π and α, so we are interested in the matrix elements of

$$\langle f|-L_x+2S_x|i\rangle.$$

The ground state is

$$|i\rangle \approx |-2, 1\rangle$$

and the excited state is

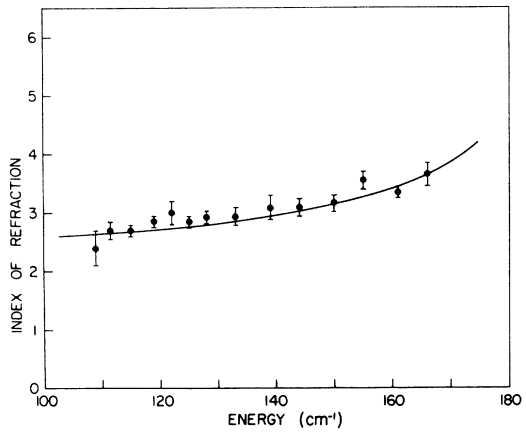

FIG. 9. Index of refraction of $FeCO_3$ at room temperature, determined from reflectivity measurements at normal incidence. The optic axis was perpendicular to the polished face of a single-crystal sample.

$$\langle f| = \alpha\langle -1, 1| - \beta\langle 0, 0| + \gamma\langle 1, -1|,$$

which yields

$$\langle f| -L_x + 2S_x|i\rangle = 2\alpha.$$

The index of refraction n was determined from reflectivity measurements made on a polished oriented crystal sample. The region 110–165 cm^{-1} was measured at room temperature and the data presented in Fig. 9 indicates $n = 2.7 \pm 0.1$ at 112.5 cm^{-1}. The rise in n toward higher energy is due to the optical phonons at 180–220 cm^{-1}. This value is close to the dc dielectric susceptibility determination of $n = 2.48$ for the isomorphic compound $CaCO_3$ (calcite).[26] By inserting the values $n = 2.7$, $\tilde{\nu} = 112.5$ cm^{-1}, the various physical constants, and the matrix element, we obtain $f_m = 4.88 \times 10^{-8}\alpha^2$. For state compositions obtained using the range of parameters determined in Sec. V, $\alpha \cong 0.8$ and thus

$$f_m = 3.1 \times 10^{-8} \text{ (calc)}.$$

The experimental determination of the oscillator strength is derived from

$$f_m = (\int \sigma d\nu)(mc/\pi e^2)(1/n).$$

The absorption cross section is defined

$$\sigma(\nu) = (-1/NL)\ln[I(\nu)/I_0(\nu)],$$

where N is the number of absorbing ions per cm^3, L is the path length of absorbing material (in cm), and $I(\nu)/I_0(\nu)$ is the relative transmitted intensity at ν. The absorption cross section is integrated in frequency space over the spectral region of the line. This can be done numerically directly from the data in Fig. 6. This procedure yields

$$f_m = 2.1 \times 10^{-8} \text{ (expt)}.$$

C. Temperature Dependence of 112.5-cm^{-1} Transition

The temperature dependence of the absorption spectra in powdered synthetic $FeCO_3$ is shown in Fig. 10. Only the frequency range near 112.5 cm^{-1} is shown since the other spectral features showed no temperature dependence. As the temperature is increased above 4.2 K there is little change in the spectrum up to about 28 K. Above this temperature the line broadens somewhat and collapses rapidly into the background as $T_N = 38$ K is approached.

This temperature dependence is consistent with what has been seen in the optical spectra of other Ising materials.[27,28] It arises from the fact that the Ising interaction permits one to describe the effective exchange field H_{ex} at an ion site to be a *discrete* sum of the exchange fields due to each neighbor. For N neighbors, the field has just $(N+1)$ possible values depending upon the "up" or "down" orientation of those neighbors. This gives rise to just $(N+1)$ possible exchange sites, each having different energy. The relative occurrence of each of these possible sites depends upon the degree of disorder of the magnetic system. In the paramagnetic phase, each single-ion electronic transition should exhibit an $(N+1)$-fold evenly spaced multiplet structure. As the temperature is lowered through the ordering temperature, the relative intensities of the components of the multiplet should change, until in the ordered state only one member remains. In a perfect Ising system, the line positions are temperature independent.

As shown by Wright *et al.*[28] for $DyPO_4$, the detailed temperature dependence of the relative intensities can be calculated using a Bethe-Peierls-Weiss (BPW) approximation on an Ising model. The predictions were very accurate for $DyPO_4$ which is known to be an excellent example of an Ising system. A similar calculation for $FeCO_3$ can, therefore, to some extent tell us how "Ising-like" it is.

The ground state of Fe^{2+} in $FeCO_3$ appears to be a good approximation of an Ising model, and we would therefore expect its possible exchange splittings to form an equally spaced multiplet. The situation in the excited state is different. In Sec. IIC, we found that in order to get the best fit to the observed transition energies and g factor, the trigonal field had to be reduced from the limiting case, resulting in a splitting of the excited-state doublet even in the absence of an exchange field. Since this splitting is of the same order of magnitude as the exchange energy, the resulting state composition is strongly dependent upon the exchange coupling. The exchange field itself is still Ising, since it arises from neighbors which are all in their ground states, and we can therefore

still describe it in terms of the orientation of the neighbors.

The observed absorption spectra will be affected in two ways by the fact that the excited state is not a good example of an Ising situation. First, the transition probabilities will no longer be independent of the exchange environment, so the BPW intensity estimates must be multiplied by the transition probability for each exchange site. Second, the excited-state exchange splittings are no longer proportional to the exchange field, but are in unequal increments, and independent of the sign of the exchange field. In order to calculate the temperature dependence, the transition probabilities and exchange splittings were obtained using the parameters in the $R = 1.0$ column of Table III. The resulting transitions are illustrated in Fig. 11, for an Ising exchange field with six neighbors. Assuming a Lorentzian line of 7-cm^{-1} width for each transition, their modified BPW temperature de-

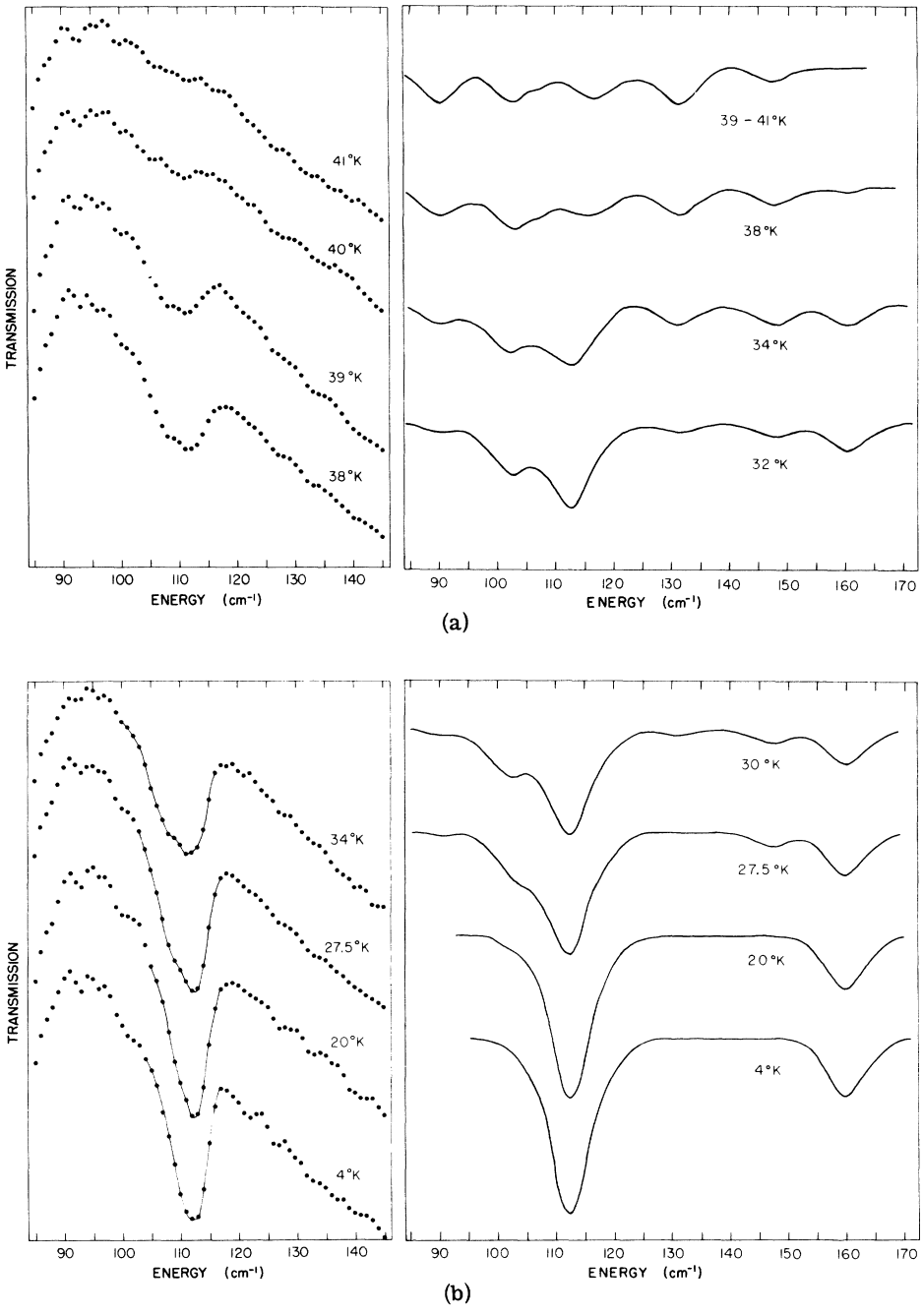

FIG. 10. Temperature dependence of the 112.5-cm^{-1} transition in a synethetic $FeCO_3$ powder sample. The experimental data points are on the left-hand side and the calculated line shapes on the right-hand side.

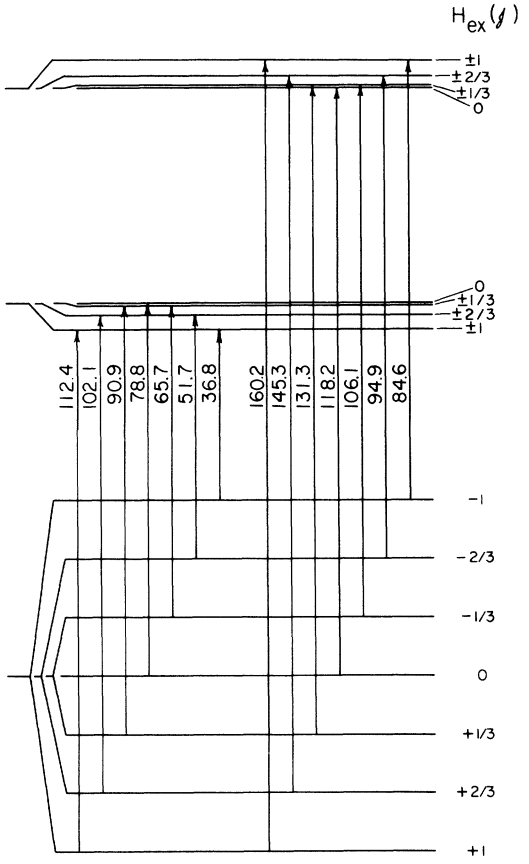

FIG. 11. Splitting of the two lowest electronic doublets by Ising exchange fields H_{ex} measured in units of the exchange parameters. At $T=0$, the maximum exchange field obtains. As the temperature is raised, the magnetic system disorders creating a distribution of ion states in progressively smaller exchange fields, as explained in the text. The allowed transitions in each of these sites is indicated. The energies given (in cm^{-1}) are obtained using the crystal-field, spin-orbit, and exchange parameters in the text.

pendence is illustrated in Fig. 10 along with the experimental data. No attempt has been made to duplicate the background detector response. The temperature discrepancies could arise from the experimental difficulties mentioned earlier. The general merging of the low-temperature line into the background is well reproduced, but the other weaker peaks predicted are not observed. This could be partly due to a general broadening with temperature, which was not included in the calculation.

Inspection of the data shows a second spectral line at 108 cm^{-1}, only 4 cm^{-1} below the 112.5-cm^{-1} line. Attempts to adjust the parameters to yield the second exchange components at this energy led to values which then did not reproduce the observed ir and Raman transitions. The 108-cm^{-1} line is present as a shoulder even at 4.2 K (see Fig. 6) and becomes relatively more prominent as the 112.5-cm^{-1} line begins to shrink. This suggests that it does not arise from disordering of the magnetic structure. According to Loudon's[29] theory of excitons, the transition does not undergo Davydov splitting, which eliminates another possible origin of doublet. Its presence in both the natural and synthetic samples dictates against it being caused by sites having a vacancy or impurity for a neighbor. Finally, it persists as a shoulder on the 112.5-cm^{-1} line even when that line is split in an applied field. This suggests that it arises from some mechanism intrinsic to the material, such as Fe^{2+} ions in some slightly altered site.

VI. CONCLUSIONS

We have presented the results of a far-infrared spectral study on natural and synthetic samples of $FeCO_3$. A single-ion model including a cubic crystalline field with a trigonal distortion, spin-orbit coupling, and an Ising exchange field is successful in describing the infrared observations in this study and the Raman data reported by others. A set of values for the spin-orbit, crystal-field, and exchange parameters has been established. The origin of the temperature-dependent doublet remains uncertain, and further investigations of the details of the exchange splittings would be useful.

ACKNOWLEDGMENTS

The authors would like to thank J. R. Weidner for supplying us with synthetic $FeCO_3$ powder. Discussions with Yu. A. Popkov and J. L. Verble, and private communications from I. S. Jacobs are gratefully acknowledged.

APPENDIX: ESTIMATES OF MAGNITUDE OF $\mathcal{J}$

A value of $\mathcal{J}$ in Eq. (3) cannot be determined directly from either infrared measurements or neutron scattering studies: The transition from $M_J=-1$ to $+1$ level of the ground exchange doublet (i.e. antiferromagnet resonance) is forbidden, and no dispersion attributable to magnons or excitons is observed. We assume the major contribution to $\mathcal{J}$ comes from nearest neighbors. If other contributions can be neglected a value for $\mathcal{J}$ may be calculated using the Bethe-Peierls-Weiss (BPW) equation,

$$kT_N=\frac{4\mathcal{J}/z}{\ln(1-2/z)}$$

for a two-sublattice Ising antiferromagnet with z-nearest neighbors. For $T_N=38.4$ K and $z=6$ this equation yields $\mathcal{J}$ (BPW) = 16 cm^{-1}. However, estimates based on BPW calculations are known to be low, so we use this number only as an estimated lower limit. An experimental number for the near-

neighbor contribution, $\mathcal{J}_{nn}$ can be determined using the measured metamagnetic transition field H_c and the Fe^{2+} magnetic moment μ. At H_c the Zeeman energy is equal to the exchange splitting due to nearest neighbors. Thus,

$$\mu H_c = z_1 J_{nn} \langle S^2 \rangle = 4\,\mathcal{J}_{nn},$$

and using $H_c = 150$ kOe and $\mu = 5\ \mu_B$, $\mathcal{J}_{nnn} \approx 19\ \mathrm{cm}^{-1}$. This is a reasonable estimate although not entirely reliable since the values of H_c and μ are somewhat uncertain.[9] It should be noted that, to first order, the value of $\mathcal{J}_{nn}$ obtained from H_c is independent of second-nearest-neighbor exchange coupling.

The second-neighbor exchange coupling $\mathcal{J}_{nnn}$ is expected to be much smaller and is more difficult to estimate. From an analysis of superexchange paths,[1] the second-neighbor coupling is predicted to be ferromagnetic, and the magnitude would therefore be added to $\mathcal{J}_{nn}$ to obtain a value for $\mathcal{J}$. Recent Monte Carlo calculations[30] fitted to experimental sublattice magnetization and T_N measurements also indicate that that the second-neighbor coupling is ferromagnetic.

There is also the optical-transmission spectroscopy by McClure *et al.*,[15] in which they have observed magnon sidebands on visible transitions. If these sidebands are caused by one-magnon excitations of $\vec{k} = 0$, the 92-cm^{-1} sideband separation implies a ground-state exchange splitting corresponding to $\mathcal{J} = 23.0\ \mathrm{cm}^{-1}$ in our notation. Of course, any dispersion in the upper electronic state involved would manifest itself in the measured sideband separation and alter this estimate. We will assume, therefore, that for the ground exchange doublet $\mathcal{J}$ is probably within the range from 16 to 23 cm^{-1}.

---

*National Research Council and Naval Research Laboratory Research Associate.

[1] I. S. Jacobs, J. Appl. Phys. 34, 1106 (1963).

[2] J. Kanamori, Prog. Theor. Phys. 20, 890 (1958).

[3] A preliminary report of this data and the analysis was presented at the Seventeenth Annual Conference on Magnetism and Magnetic Materials, Chicago, 1971 (see Ref. 14).

[4] R. W. G. Wycoff, *Crystal Structures* (Interscience, New York, 1964), Vol. II, p. 362.

[5] M. Foex, Ann. Phys. 16, 174 (1921); H. Bizette, J. Phys. Radium 12, 161 (1951).

[6] R. A. Alikhanov, Sov. Phys. JETP 9, 1204 (1959).

[7] N. F. Kharchenko, L. I. Beliy, and V. V. Eremenko, Izv. Akad. Nauk SSSR, Ser. Fiz. 36, 1230 (1972).

[8] I. S. Jacobs, S. Roberts, and P. E. Lawrence, J. Appl. Phys. 36, 1197 (1965); A. Ito and K. Onon, J. Phys. Soc. Jap. 20, 784 (1965).

[9] In a private communication, I. S. Jacobs has provided us with his unpublished magnetization data on a natural single crystal from Greenland which is of higher purity than his previous work (Ref. 1). For external magnetic fields applied parallel to the C_3 axis the magnetization shows a sharp jump near 150 kOe. We take this to be the metamagnetic transition although the transition is quite broad. At a pulsed field of 270 kOe the magnetization reaches a value of 220 emu/g but is still increasing, This magnetization corresponds to an Fe^{2+} magnetic moment of $4.65\mu_B$. However, a saturated magnetization of 241 emu/g, corresponding to $5\mu_B$ per Fe^{2+} ion is not at all an unreasonable extrapolation of his data.

[10] D. W. Forester and N. C. Koon, J. Appl. Phys. 40, 1316 (1969).

[11] H. N. Ok, Phys. Rev. 185, 472 (1969).

[12] D. E. Wrege, S. Spooner, and H. A. Gersch, AIP Conf. Proc. 5, 1334 (1972).

[13] A. Okiji and J. Kanamori, J. Phys. Soc. Jap. 19, 908 (1964).

[14] G. A. Prinz and D. W. Forester, in Ref. 12, p. 279.

[15] D. S. McClure, R. Meltzer, S. A. Reed, P. Russell, and J. W. Stout, in *Optical Properties of Ionic Crystals*, edited by H. M. Crosswhite and H. W. Moss (Interscience, New York, 1967), p. 257.

[16] Yu. A. Popkov, V. V. Eremenko, V. I. Fomin, and A. P. Mokhir, Fiz. Tverd. Tela. 14, 1985 (1973) [Sov. Phys.-Solid State 14, 2294 (1972)].

[17] D. B. Langille and D. C. O'Shea, Bull. Am. Phys. Soc. 17, 269 (1972).

[18] C. J. Ballhausen, *Introduction to Ligand Field Theory* (McGraw-Hill, New York, 1962), p. 103.

[19] This estimate follows from the analysis of Okiji and Kanamori (Ref. 13) and an extension of this analysis by M. Eibschütz, U. Ganiel, and S. Shtrikman [Phys. Rev. 151, 245 (1966)].

[20] R. J. Birgeneau, W. B. Yelon, E. Cohen, and J. Makovsky, Phys. Rev. B 5, 2607 (1972).

[21] J. S. Griffith, *The Theory of Transition-Metal Ions* (Cambridge U. P., Cambridge, Mass., 1961), p. 357.

[22] Fourier Spectrophotometer, Model No. 720 manufactured by Research and Industrial Instruments Corp., London, England.

[23] A description of this detector was given at the IRIS Conference held at Naval Research Laboratory, Washington, D. C., March, 1973 (unpublished).

[24] The synthetic, powdered $FeCO_3$ was supplied to us by J. R. Weidner, Dept. of Geology, University of Maryland at College Park. Emission analysis revealed less than 0.001-at.% transition-metal impurity and less than 0.014-at.% total impurity level.

[25] K. H. Hellwege, W. Lesch, M. Plihal, and G. Schaack, Z. Phys. 232, 61 (1970).

[26] *Handbook of Chemistry and Physics* (The Chemical Rubber Co., Cleveland, 1967), p. E60.

[27] G. A. Prinz, Phys. Rev. 152, 474 (1966).

[28] J. C. Wright, H. W. Moos, J. H. Colwell, B. W. Mangum, and D. T. Thornton, Phys. Rev. B 3, 843 (1971).

[29] R. Loudon, Adv. Phys. 17, 243 (1968).

[30] R. F. Altman, S. Spooner, and D. P. Landau, AIP Conf. Proc. 10, 1163 (1972).